Cell, Vol. 121, 1005–1016, July 1, 2005, Copyright ©2005 by Elsevier Inc. DOI 10.1016/j.cell.2005.04.024

Crystal Structures of RNase H Bound to an RNA/DNA Hybrid: Substrate Specificity and Metal-Dependent Catalysis

Marcin Nowotny,[1] Sergei A. Gaidamakov,[2] Robert J. Crouch,[2] and Wei Yang[1,*]
[1]Laboratory of Molecular Biology
National Institute of Diabetes and Digestive and Kidney Diseases
[2]Laboratory of Molecular Genetics
National Institute of Child Health and Human Development
National Institutes of Health
Bethesda, Maryland 20892

Summary

RNase H belongs to a nucleotidyl-transferase superfamily, which includes transposase, retroviral integrase, Holliday junction resolvase, and RISC nuclease Argonaute. We report the crystal structures of RNase H complexed with an RNA/DNA hybrid and a mechanism for substrate recognition and two-metal-ion-dependent catalysis. RNase H specifically recognizes the A form RNA strand and the B form DNA strand. Structure comparisons lead us to predict the catalytic residues of Argonaute and conclude that two-metal-ion catalysis is a general feature of the superfamily. In nucleases, the two metal ions are asymmetrically coordinated and have distinct roles in activating the nucleophile and stabilizing the transition state. In transposases, they are symmetrically coordinated and exchange roles to alternately activate a water and a 3′-OH for successive strand cleavage and transfer by a ping-pong mechanism.

Introduction

RNase H (RNase HI) is a sequence-nonspecific endonuclease that cleaves RNA strands in RNA/DNA hybrids. The main cellular function of RNase H is to remove RNA primers from Okazaki fragments and process R loops to modulate replication initiation and restore DNA topology (Broccoli et al., 2004; Kogoma and Foster, 1998). In unicellular organisms, the RNase H function is redundantly encoded, and *rnh* null mutants survive (Arudchandran et al., 2000). In contrast, RNase H knockout mice die in embryo at day 8.5 due to the lack of mitochondrial DNA synthesis (Cerritelli et al., 2003). In retroviruses, RNase H activity is encoded as a part of the reverse transcriptase (RT) that converts a retroviral single-stranded RNA (ssRNA) genome into dsDNA (Hughes et al., 1998). In addition to removal of the template RNA after synthesis of a complementary DNA strand, RNase H has other roles, including production of a polypurine primer for the second-DNA-strand synthesis. Mutations that abolish either polymerase or RNase H activity of RT prevent viral replication (Repaske et al., 1989; Tisdale et al., 1991). RNase H is also an essential component of the antisense technique that degrades mRNA and reduces gene expression (Wu et al., 2004).

Crystal structures of *E. coli* RNase H were first determined in 1990 and revealed a novel α/β fold containing a carboxylate triad in the catalytic center (Katayanagi et al., 1990; Yang et al., 1990). A similar fold and related active sites have since been found in RNase HII (Lai et al., 2000), RuvC (a Holliday junction resolvase) (Ariyoshi et al., 1994; Ceschini et al., 2001), DNA transposases, and retroviral integrases (Rice and Baker, 2001). Most recently, the protein component of an RNA-induced silencing complex (RISC) was found to contain an RNase H-like domain essential for degrading RNA in siRNA (Parker et al., 2004; Song et al., 2004; Figure 1A). These enzymes play important roles in a wide range of cellular and retroviral functions and in gene therapy, but the mechanism for substrate recognition and metal-dependent catalysis remains in question. To date, only a bacterial DNA transposase (Tn5) has been crystallized in complex with a nucleic-acid substrate (Davies et al., 2000; Steiniger-White et al., 2004). Crystal structures of RT complexed with a dsDNA or RNA/DNA hybrid have captured the substrate only in the polymerase but not the RNase H active site (Huang et al., 1998; Sarafianos et al., 2001). Despite continuous efforts since 1990, a crystal structure of RNase H complexed with an RNA/DNA substrate remains elusive.

In nucleotidyl transfer reactions catalyzed by an RNase H-like enzyme, the nucleophile is derived from either a water molecule or a 3′-OH of nucleic acid. Transposases and retroviral integrases, which catalyze at least two sequential reactions, donor-end processing and strand transfer, possess three conserved carboxylates (two Asps and one Glu) in the active site, known as the DDE motif (Haren et al., 1999; Figure 1A). The two conserved Asps are characteristically located at the fork of a pair of long and short parallel β strands. These Asps are also found in the active sites of RNase H, RNase HII, and Argonaute in the same spatial configuration. In RNase H (both I and II), the C-terminal carboxylate of the acidic motif is an Asp, and both enzymes contain an additional catalytically essential carboxylate, a Glu between the two spatially conserved Asps (Figure 1A).

The carboxylate-rich and negatively charged active site of an RNase H-transposase-like enzyme depends on divalent cations, Mg^{2+} or Mn^{2+}, to bind substrate and catalyze nucleotidyl transfer reactions. Based on stereochemical studies, reactions catalyzed by these enzymes occur by a one-step S_N2-like (bimolecular nucleophilic substitution) mechanism accompanied by a pentacovalent intemediate and inversion of the phosphate stereo configuration (Kennedy et al., 2000; Krakowiak et al., 2002). A two-metal-ion catalysis mechanism was proposed, with one metal ion activating the hydroxyl nucleophile and the other stabilizing the pentacovalent intermediate (Steitz and Steitz, 1993). This proposal was supported by the crystal structure of Tn5 transposase-DNA complexes, in which two metal ions are coordinated by the DDE motif in the active site (Lov-

*Correspondence: wei.yang@nih.gov

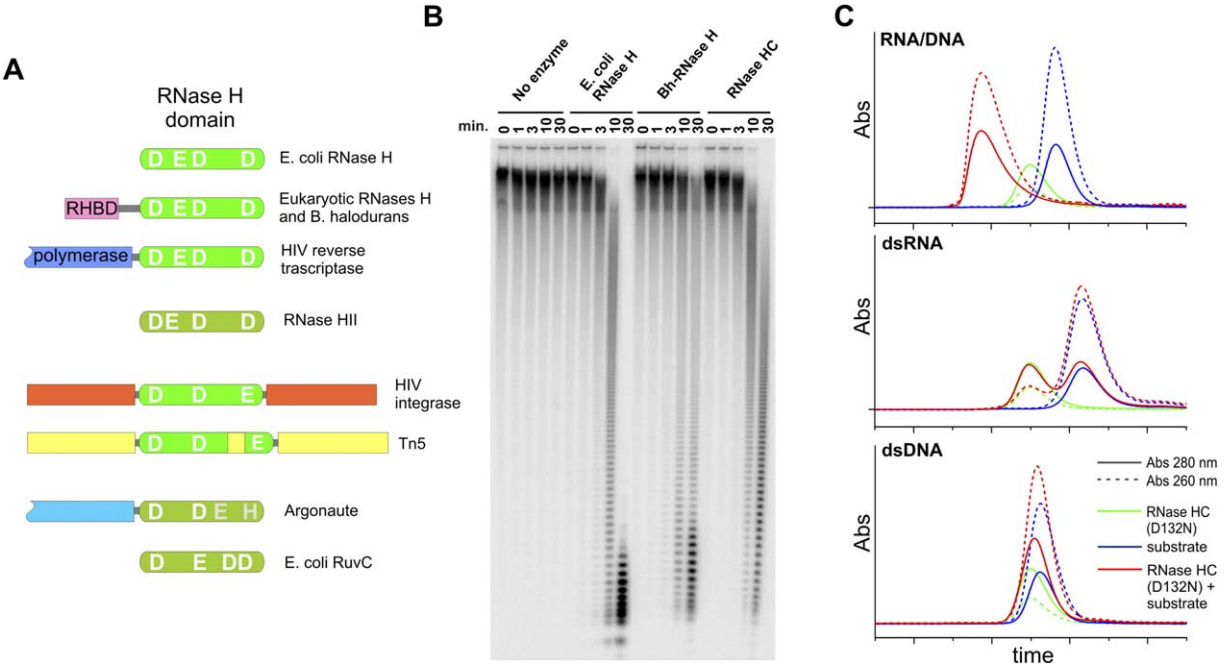

Figure 1. Active Site of RNase H and Its Relatives

(A) Domain alignment of selected members of the polynucleotidyl transferases. The known active-site residues are labeled in white, the predicted in gray.

(B) RNase H activity assay. Each protein was incubated with uniformly ^{32}P-labeled poly(rA)/poly(dT) for indicated times. The products were resolved on a polyacrylamide sequencing gel.

(C) Substrate binding assay. Elution profiles of *Bh*-RNase HC(D132N) protein (green), RNA/DNA hybrid, dsRNA or dsDNA (blue), and the mixture of the protein and nucleic acid at a 2:1 molar ratio (red) from a Superdex-75 column are superimposed. The protein-RNA/DNA complexes are eluted before the protein or nucleic acid alone.

ell et al., 2002). However, two metal ions were observed in the apo-RNase H active site only when Mg^{2+} concentrations exceeded 10 mM. Mysteriously, many RNases H lose their activity at such high concentrations of divalent cations, which led to the "attenuation model" proposing that binding of the first metal ion activates the enzyme and binding of the second leads to its inhibition (Goedken and Marqusee, 2001; Keck et al., 1998). Repeated observations of a single metal ion bound in the RNase H active site have led to various hypotheses of one-metal-ion catalysis (Oda et al., 1993; Tsunaka et al., 2005). As shown in the Tn5 case, however, binding of metal ions may depend on the presence of a nucleic-acid substrate. In the absence of substrate, the number of metal ions required for enzymatic activity and their locations cannot be conclusively determined from X-ray structures.

Substrate recognition by members of this nucleotidyl-transferase superfamily has been even less well understood. Despite a conserved active site, substrates are dramatically different. RuvC recognizes a Holliday junction and resolves it to two DNA duplexes; transposase and retroviral integrase recognize specific sequences at donor-DNA ends, cleave the ends from flanking sequences, and insert them into a new target site; Argonaute recognizes an RNA duplex formed between an ~20-mer and a longer strand and cleaves the longer one in the middle of the duplex region. Crystallographic studies of RNA/DNA hybrids suggest that they adopt an A form conformation (Kopka et al., 2003) common to both dsRNA and dsDNA. How does RNase H then discriminate against dsRNA and dsDNA? The last but certainly not the least important question is how transposases and integrases are able to catalyze DNA hydrolysis and strand transfer using the same active site (Bolland and Kleckner, 1996; Kennedy et al., 2000).

We have succeeded in crystallizing a bacterial RNase H and two catalytically deficient forms complexed with RNA/DNA hybrids. These crystal structures reveal the atomic arrangement of the active site and the mechanisms for substrate recognition and metal-ion-dependent RNA hydrolysis. Comparisons of the available structures in the nuclease-transposase superfamily suggest a conserved two-metal-ion catalytic mechanism. We propose that, in DNA transposition, both metal ions play catalytic roles and alternately activate a water molecule or a 3′-OH for successive DNA hydrolysis and strand transfer.

Results and Discussion

Biochemical and Structural Characterization of *B. halodurans* RNase H

To obtain crystals of an RNase H complexed with its substrate, we examined five homologs from mammals, fungi, archaea, and bacteria, each of which contains a ds*R*NA and RNA/DNA *h*ybrid *b*inding *d*omain (RHBD) N-terminal to the catalytic domain. RNase H from *Bacillus halodurans* (196 aa), which contains the shortest linker (10 aa) between the RHBD and RNase H do-

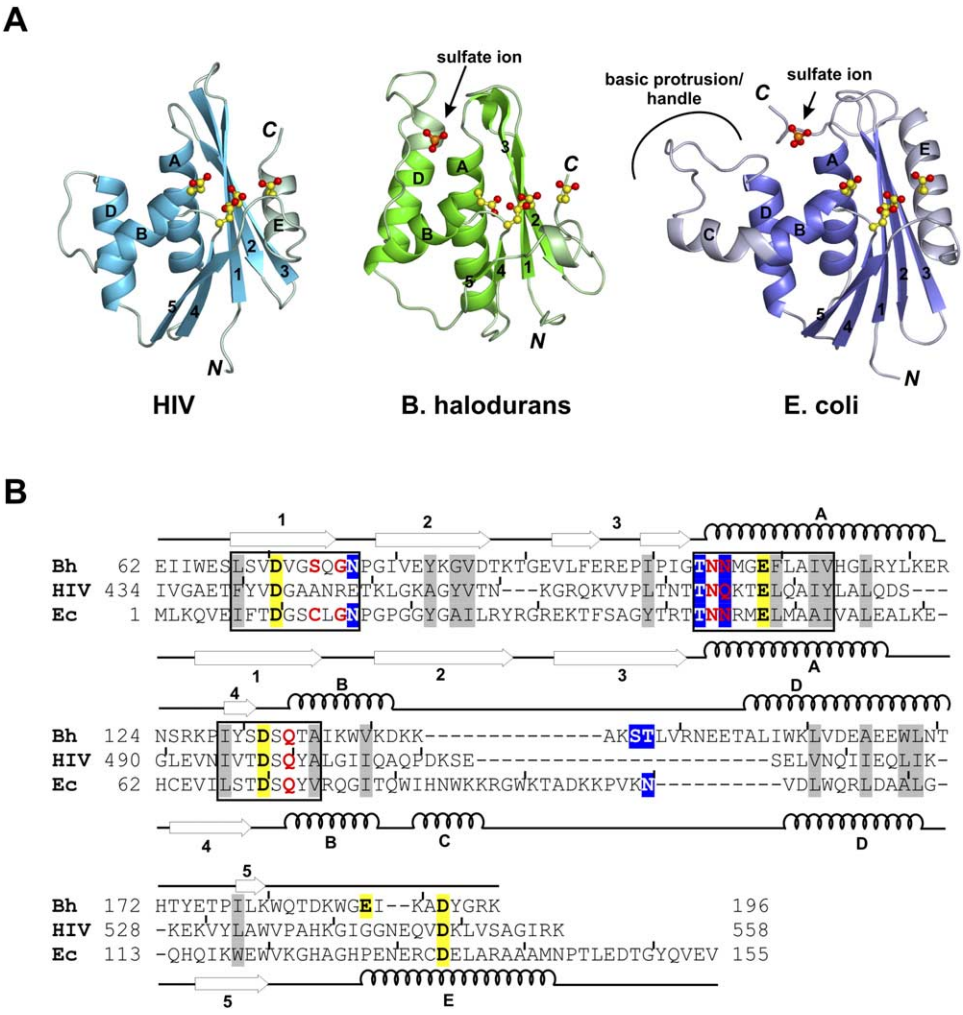

Figure 2. Structure and Sequence Comparison of *Bh*, *E. coli*, and HIV RNases H

(A) Ribbon diagrams of HIV (PDB ID code 1RTD), *Bh*, and *E. coli* (PDB code 1RNH) RNases H. The conserved structural core is shown in darker color in each case. The active-site carboxylates are shown as yellow (carbon) and red (oxygen) ball-and-stick models, and the sulfate ions are shown as orange and red ball-and-stick models.

(B) Sequence alignment of the three RNases H. Secondary structures of *Bh* and *E. coli* RNases H are indicated above and below the corresponding sequences. Residues that contact the RNA strand are labeled in red, those contacting DNA are highlighted in blue, and the residue contacting both RNA and DNA is shown as red on blue. Conserved hydrophobic-core residues are highlighted in gray. The three conserved regions are boxed.

mains, gave the best results in expression and solubility tests. Both the full-length protein and the C-terminal *Bh*-RNase H domain alone (RNase HC) are stable in solution and possess RNase H activity (Figure 1B). Mutations of the conserved carboxylates, E109 or D132, which are equivalent to E48 and D70 of *E. coli* RNase H (Figure 2), inactivate *Bh*-RNase H (see below). Fortuitously, the D132N mutant RNase HC binds RNA/DNA hybrids better than the wild-type form, and the binding is specific for hybrids and not dsDNA or dsRNA (Figure 1C).

After exhaustive trials, the full-length *Bh*-RNase H gave no crystals, but RNase HC(D132N) (59–196 aa) crystallized in both the apoprotein form as well as in complex with a 12 bp RNA/DNA hybrid. The apoprotein structure was solved using selenomethionine substitution and the multiwavelength anomalous diffraction method (Hendrickson et al., 1990). The refined model consists of residues 62 to 193. The substrate-complex structure was solved using molecular replacement and refined using CNS (Brunger et al., 1998). Data collection and refinement statistics are shown in Table 1. Two RNase HC molecules are associated with each 12 bp hybrid as suggested by the gel filtration analyses (Figure 1C). Each protein molecule (I and II, traceable to residues 196 and 194, respectively) binds one half of the substrate without direct protein-protein contact (Figure 3), and the two halves of the complex are basically identical.

The RNase H Structure

The structures of RNase HC with or without substrate are superimposable with root-mean-square deviations (rmsds) of 0.5–0.6 Å over 120 pairs of Cα atoms. Differ-

Table 1. Data Collection and Refinement Statistics

MAD Data Statistics, Apoprotein			
Space group	$P3_121$		
Wavelength (Å)	0.9700	0.9793	0.9796
Resolution range (Å)[a]	30–1.8 (1.86–1.80)		
Completeness (%)[a]	99.7 (98.0)	99.3 (95.2)	97.7 (79.5)
R_{merge}[a,b]	0.076 (0.278)	0.071 (0.230)	0.080 (0.344)
$I/\sigma(I)$[a]	26.5 (4.9)	29.7 (5.3)	23.4 (2.9)
Figure of merit: 0.54 (30.0–2.0 Å) (determined by SOLVE)			
Refinement	**Apoprotein**	***Bh*-RNase HC(D132N) Complex**	***Bh*-RNase HC(D192N) Complex**
Space group	$P3_121$	C2	P1
Unit cell a, b, c (Å)	66.8, 66.8, 58.7	136.4, 37.0, 93.2	36.9, 45.0, 62.3
α, β, γ (°)	90, 90, 120	90, 121.5, 90	83.6, 89.9, 65.7
Resolution range (Å)[a]	30–1.5 (1.55–1.50)	30–1.85 (1.92–1.85)	30–2.2 (2.28–2.2)
Completeness (%)[a]	98.5 (97.7)	91.4 (55.6)	89.3 (56.3)
R_{merge}[a,b]	0.056 (0.417)	0.048 (0.352)	0.047 (0.325)
$I/\sigma(I)$[a]	35.1 (2.7)	25.5 (1.8)	17.1 (2.0)
Unique reflections	23,577	29,836	15,213
Nonhydrogen atoms	1337	2944	3286
R value[c]	0.189	0.206	0.217
R_{free}[d]	0.214 (1141)	0.248 (1474)	0.253 (1489)
Rmsd bond length (Å)	0.008	0.007	0.007
Rmsd bond angle (°)	1.346	1.291	1.086
Average B value ($Å^2$)	19.7	29.4	41.1
ϕ, ψ distribution (%)[e]	94.0/6.0	91.6/8.4	89.3/10.7

[a] Data of the highest resolution shell is shown in parentheses.
[b] $R_{merge} = \Sigma_h\Sigma_i |I_{hi} - \langle I_h\rangle|/\Sigma\langle I_h\rangle$, where I_{hi} is the intensity of the i^{th} observation of reflection h and $\langle I_h\rangle$ is the average intensity of redundant measurements of the h reflections.
[c] R value = $\Sigma||F_o| - |F_c||/\Sigma|F_o|$, where F_o and F_c are the observed and calculated structure-factor amplitudes.
[d] R_{free} is monitored with the number of reflections in parentheses excluded from refinement.
[e] Residues in the most favored and additionally allowed regions of the Ramachandran plot.

ences exist in the C terminus and the loop between β1 and β2, which undergoes the largest change between the apo and substrate bound structure (2.5 Å at the Cα of N77). The tertiary structure is homologous to that of *E. coli* RNase H and consists of a mixed β sheet with three antiparallel (1, 2, and 3) and two parallel (4 and 5) strands and three α helices (A, B, and D) arranged like a letter "H" on one side of the sheet (Figure 2A). Helix A runs between strands 3 and 4, and helices B and D run between strands 4 and 5. Together they form the αβα Rossmann-like fold.

Comparison of the three classes of RNase H, *E. coli* (stand-alone catalytic domain), *B. halodurans* (with RHBD), and HIV (with polymerase), reveals a conserved ~100-residue core structure consisting of the five-stranded β sheet and three α helices (A, B, and D) (Fig-

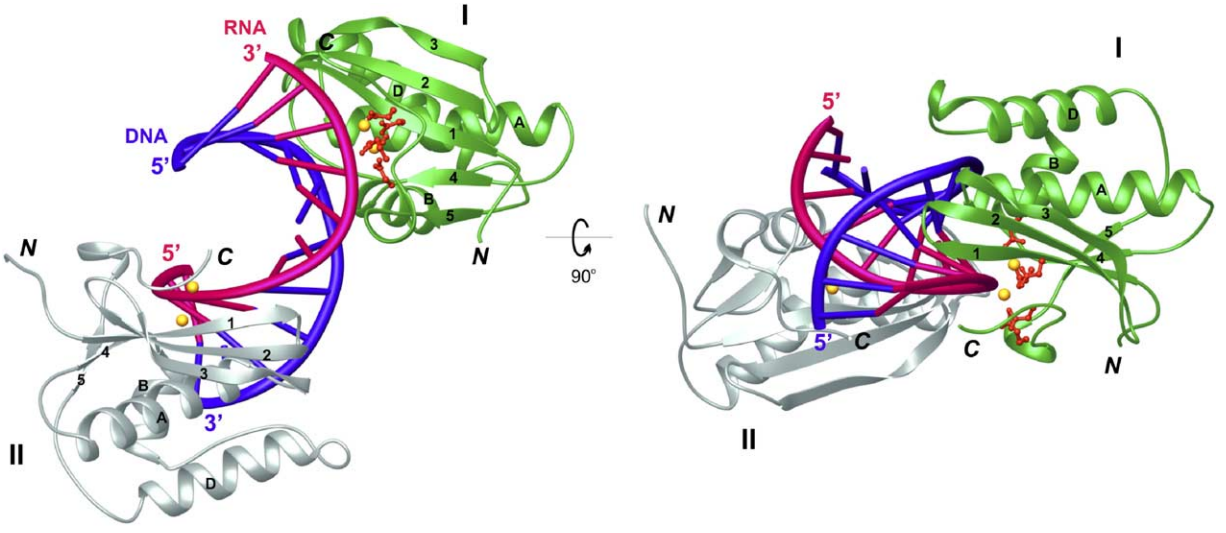

Figure 3. *Bh*-RNase HC Complexed with an RNA/DNA Hybrid

Two protein molecules, RNA, and DNA are color coded and shown in ribbon diagrams. The carboxylates in the active site are shown as red sticks and the two magnesium ions as yellow spheres.

ure 2A). Helix C and the basic protrusion or "handle" is unique to the *E. coli* structure. The basic protrusion, which has been implicated in substrate binding by *E. coli* RNase H (Haruki et al., 1997), may be functionally replaced by RHBD in *Bh*-RNase H and the polymerase domain in RT. Additional differences are found at the C terminus, which is the shortest in *B. halodurans* and longest in *E. coli*. A hydrophobic patch exposed by the shortened C-terminal end in *Bh*-RNase H is covered by the lengthened and reoriented helix D (Figure 2A). Despite the absence of the entire helix E in *Bh*-RNase H, the fourth conserved carboxylate (D192) is present on an extended loop and superimposable with D134 of the *E. coli* RNase H and D549 of HIV RT on the E helix (Figure 2).

The Mixed A and B Form RNA/DNA Hybrid and Substrate Specificity of RNase H

The RNA/DNA hybrid in the complex of RNase HC adopts a mixed A and B conformation. The RNA strand is in A form with 3′-endo sugar puckers, and the DNA strand is in B form with 2′-endo or 1′-exo sugars. This mixed conformation is similar to the NMR structures of protein-free RNA/DNA hybrids (1EFS, 124D, 1RRD) but differs from the A-like structures determined by crystallography (1FIX, 1PJG, 479D). In addition to the sugar puckers, the mixed A and B character of RNase HC substrate is reflected in the minor-groove width. The average minor-groove width of three A-like crystal structures of RNA/DNA hybrids is 9.8 Å, and the average of three mixed A/B form NMR structures is 8.4 Å, which is the same as that in the RNase HC complex (Figure 4A). Superposition of the three crystal and three NMR structures of RNA/DNA hybrids with that of the RNase HC complex reveals a near perfect alignment of the RNA strands, but the positions of the DNA strands differ (Figure 4B). The B form DNA strand with one local distortion fits the RNase HC surface perfectly, while the A-like structure does not. RNases H probably select and stabilize an RNA/DNA hybrid in the mixed A and B conformation and thereby discriminate against dsRNAs, which are invariably A form.

Specificity for the RNA strand is determined by direct contacts between RNase HC and five consecutive 2′-OH groups (Figure 4C). The face of the RNase HC containing the active site has two grooves separated by ~8.5 Å, into which the backbones of the RNA/DNA hybrid fit snugly, with the minor groove straddling the ridge in between (Figure 4B). Upon the association of RNase HC and a 6 bp RNA/DNA hybrid, ~1000 Å of molecular surface becomes buried, which is similar to the typical interface between an antibody and antigen. The active site of RNase H is located in the groove that accommodates the RNA strand. The catalytic carboxylates E109, D132(N), and their immediate neighbors (N106 and Q134) make hydrogen bonds with two 2′-OH groups immediately 5′ to the scissile phosphate. S74 and G76 adjacent to D71 (the other active-site residue) contact the two 2′-OH groups 3′ to the scissile phosphate. The contact between Q134 and the fifth 2′-OH occurs only in molecule I and not II and may be sequence dependent. The recognition of the 2′ hydroxyl groups is likely conserved in all RNases H since the residues surrounding D71, E109, and D132 are highly conserved (Figure 2B). These contacts explain why cleavage of a chimeric DNA-RNA-DNA/DNA by *E. coli* RNase H requires a minimum of four riboses, two on each side of the scissile bond (Ohtani et al., 1999).

The DNA binding groove, which comprises the N terminus of helix αA and the loops between helices αB and αD and between the β1 and β2 strands (Figure 3), is accentuated by a phosphate binding pocket composed of T104, N106, S147, and T148. In the apoprotein structure, this pocket is occupied by a tightly bound sulfate ion (Figure 4D). The sulfate ion is perfectly replaced by the DNA phosphate two base pairs away from the scissile bond in the protein-substrate complex (Figure 4E). Interestingly, a sulfate ion was originally found in the *E. coli* RNase H structure at an analogous position (Figure 2A) and was hypothesized to mimic the DNA backbone (Yang et al., 1990). Around the phosphate binding pocket, the DNA backbone is distorted (Figure 4B), and the minor groove is narrowed (Figure 4A). The C5′-C4′ (γ) and P-O5′ (α) torsion angles of the phosphate deviate from the ideal values by nearly 180°. Two out of the four coordination ligands for the sulfate ion, TN(N/Q) at the N terminus of helix A, are conserved throughout RNases H. Mutations of these two phosphate ligands (T43 and N45 in *E. coli* and T473 and Q475 in HIV RT) result in great reduction of RNase H activity and blockage of viral replication (Julias et al., 2002; Kanaya, 1998). The remaining two ligands in *Bh*-RNase H (S147 and T148) are partially replaced by N100 in *E. coli* RNase H but are absent in HIV RT. The extra sulfate/phosphate ligand may enable *Bh*-RNase H to bind substrate better than other homologs. With only two sulfate/phosphate ligands, HIV RT can cleave dsRNA as well as RNA/DNA hybrids under certain conditions (Gotte et al., 1995; Hughes et al., 1998). The phosphate binding pocket probably plays a role in anchoring the B form DNA and contributes to the specificity for an RNA/DNA hybrid.

In addition to interacting with RNA and DNA backbones, N77, N105, N106, and Q134 donate hydrogen bonds to bases in the minor groove (Figures 2B and 4C). These four residues are conserved perhaps for maintaining the RNase H tertiary structure (N77 and N105) and contacting the 2′-OH of RNA (Q134). Mutation of the equivalents of N77 or Q134 in *E. coli* RNase H (N16 and Q72, Figure 2B) to Ala dramatically increases the K_M (Kanaya, 1998). Notably, a sequence-specific contact occurs in the major groove between the guanidinium group of R195 and a guanine at the D+5 position of an end-to-end-stacked neighboring DNA. Basic residues equivalent to R195 exist in *E. coli* (R138) and HIV RNase H (R557) and may favor a guanine 5–6 bp 3′ to the scissile bond.

The Active-Site Configuration and Two-Metal-Ion Catalysis

The four conserved carboxylates, D71, E109, D132, and D192 in RNase HC, are directly involved in coordinating the metal ions. Two Mg^{2+} ions were found in the active site of the substrate complex even though only 2.5 mM $MgCl_2$ was present in the crystallization buffer and $MgCl_2$ was omitted in the cryoprotection solutions. The dissociation constant for the two Mg^{2+}, therefore, has

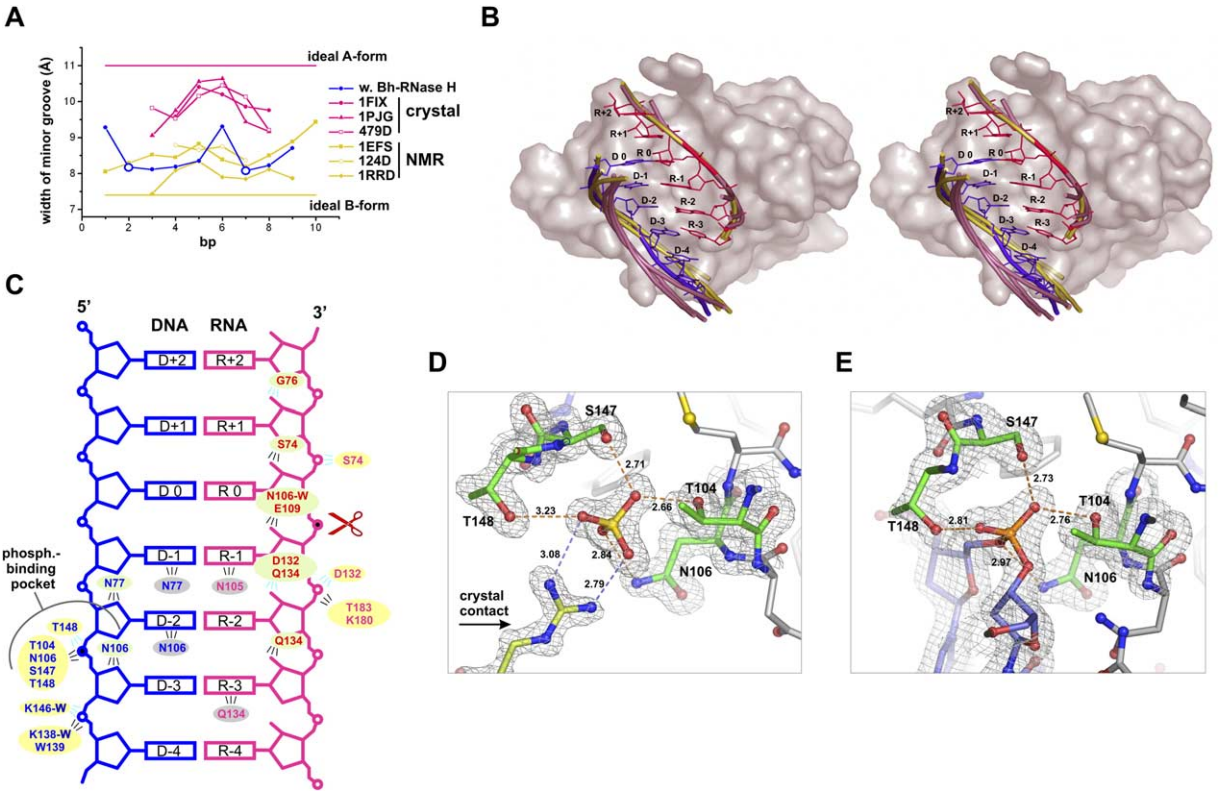

Figure 4. The RNA/DNA Hybrid and Its Interactions with *Bh*-RNase HC

(A) Plot of the minor-groove width of the hybrids in the crystal (pink lines), NMR (yellow lines), and RNase HC structures (blue line). Phosphates in the phosphate binding pocket are indicated by open circles.

(B) Stereoview of the RNase HC-substrate complex. The molecular surface of RNase HC is shown in pinkish gray, and the substrate RNA (red) and DNA (blue) are shown as rods (backbone) and sticks (bases). The three crystal (pink) and three NMR (yellow) structures of RNA/DNA hybrids are superimposed onto the RNase HC structure. Nucleotides are numbered relative to the nucleotide at the active site (R 0) and according to the polarity of the RNA strand.

(C) Interactions between the RNA/DNA hybrid and RNase HC. Shown are the residues interacting with phosphates (yellow highlight), sugars (green highlight), and bases (gray highlight). Cyan lines indicate interactions made by the protein backbone, and black lines indicate interactions made by side chains. Water-mediated interactions are indicated by -W.

(D and E) The phosphate binding pocket in the apo (D) and the substrate-complex (E) structure. The hydrogen bonds with the sulfate or phosphate are indicated by dashed orange lines. A $2F_o - F_c$ omit map contoured at 1.5 σ is superimposed over the structure model.

to be significantly below 2.5 mM. In apoprotein crystals grown at the same Mg^{2+} concentration, no metal ion was found at the active site (data not shown).

The first conserved carboxylate, D71, is located in the middle of the β1 strand and coordinates both metal ions A and B (Figure 5A). The A metal is also coordinated by D192, E188 (a nonconserved fifth carboxylate), the pro-S_p oxygen atom of the scissile phosphate, and two water molecules in a nearly perfect octahedral geometry (Figure 5A). One of the water molecules is 3.4 Å away from the scissile phosphate and is perfectly positioned for an in-line nucleophilic attack. This water molecule does not contact any protein residues, but it is only 3 Å from the pro-R_p oxygen of the phosphate immediately 3′ to the scissile bond. Replacement of this pro-R_p but not the pro-S_p oxygen with a sulfur atom reduces the k_{cat} of *E. coli* RNase H by 86% (Haruki et al., 2000). This pro-R_p oxygen most likely orients the water for the nucleophilic attack and may even serve as a general base for deprotonation and then shuttle the proton to solvent.

The B metal ion, which is expected to stabilize the pentacovalent intermediate and the product 3′-OH, is coordinated by E109, D132 (mutated to Asn), and both bridging and nonbridging oxygen atoms of the scissile phosphate (Figure 5A). Its coordination geometry deviates significantly from an ideal octahedron, perhaps due to the nature of a substrate complex rather than the transition state and also the D132N substitution. As D132N appears only to affect the coordination of metal B, we were puzzled as to why replacing this carboxylate with a carboxylamide completely inactivates the RNase H activity (Figure 5D).

We made the D192N mutation, which inactivates *Bh*-RNase H (Figure 5D) but leaves the coordination of the B metal intact. The mutant protein was crystallized in complex with the same RNA/DNA hybrid in a different space group (Table 1). There are again two protein molecules bound to one 12 bp hybrid. Except for a 1 bp shift of one protein molecule, the overall protein structure and protein-nucleic-acid interactions remain the same as in the D132N mutant. However, the following

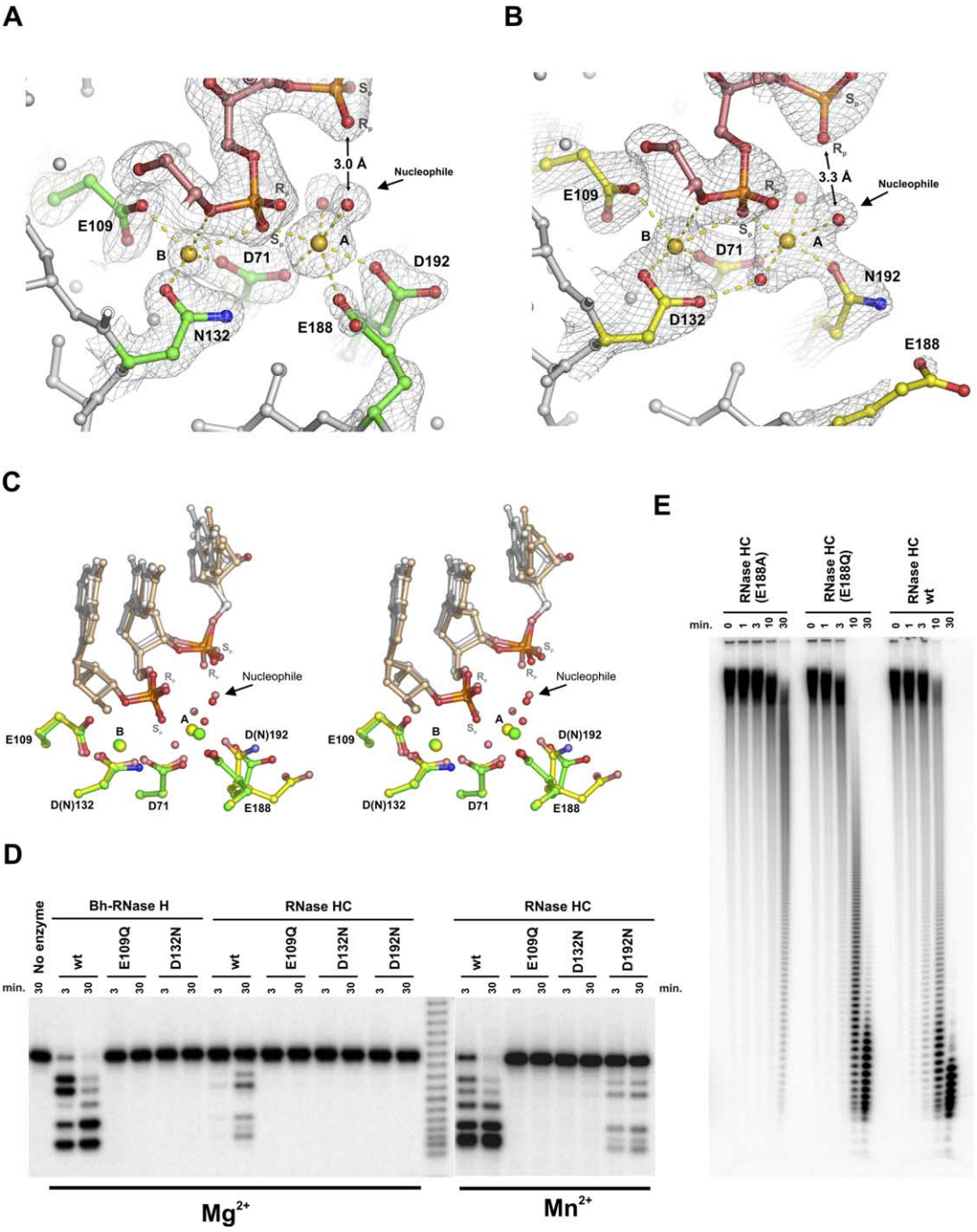

Figure 5. The Active Site

(A and B) The active site of D132N (A) and D192N (B) in complex with the RNA/DNA hybrid. Active-site residues are shown in green (D132N) or yellow (D192N); the RNA strand in pink, orange, and red; and the magnesium ions as yellow spheres. The water molecule positioned to attack the scissile phosphate is indicated. Metal-ion coordination is shown as dashed yellow lines. A $2F_o - F_c$ omit map contoured at 1.5 σ is also shown. Pro-R_p and pro-S_p oxygens are labeled as R_p and S_p, respectively.

(C) Stereoview of the superimposed active sites of the D132N (green for the protein carbon atoms and magnesium ions and pink for sugars and bases) and D192N (yellow for the protein carbon atoms and magnesium ions and gray for sugars and bases).

(D) Hydrolysis of the 12-mer RNA/DNA hybrid by wild-type and mutant *Bh*-RNase H. Cleavage of the ^{32}P-labeled substrate was monitored in the presence of 5 mM $MgCl_2$ or 20 mM $MnCl_2$.

(E) Activity of the E188 mutant proteins. Uniformly ^{32}P-labeled poly(rA)/poly(dT) was cleaved by wild-type, E188Q, or E188A RNase HC.

changes are observed in the active site and reveal much about the metal-ion coordination and RNase H catalytic mechanism. In the D192N structure, D132 not only directly coordinates metal B but also coordinates metal A via a water molecule, displacing E188 as an A metal-ion ligand (Figures 5B and 5C). D71 and D132, the two Asps spatially conserved in RNases H and HII, Argonaute, transposases, and integrases, are thus involved in the coordination of both metal ions.

The Mg^{2+} at the B site is secluded from bulk solvent and has a relatively fixed position due to coordination by three conserved carboxylates (D71, E109, and D132) and the scissile phosphate. The Mg^{2+} at the A site, although linked to the hydroxyl nucleophile and ideally coordinated, shifts its position and is closer to the B metal in the D192N complex (4.1 Å) than in the D132N complex (4.4 Å). Replacement of D192 by Asn inactivates RNase H in the presence of Mg^{2+}, but Mn^{2+} partially restores the catalytic activity (Figure 5D). In contrast, the D132N mutant RNase H has no detectable activity with either Mg^{2+} or Mn^{2+} (Figure 5D). The larger Mn^{2+} may shift the A site a little further away from the B site and thus compensate for the shortened distance between the two metal ions in the case of D192N. But in the case of the D132N, the greater separation between the metal ions would be even greater with Mn^{2+} and cannot be reversed.

We conclude that both metal ions are essential and must be correctly positioned for catalysis. The distance between the two is determined by the configuration of the active-site carboxylates and substrate. E109, which directly contacts a 2′-OH of the RNA backbone and is surrounded by residues interacting with the DNA strand (Figure 4C), has the largest shift at the Cα (0.4 Å) among the four conserved carboxylates compared to the apo structure. The influence of substrate on the metal-ion coordination ensures the catalytic specificity of RNases H. Replacing Mg^{2+} with Mn^{2+}, known for relaxed coordination geometry, not only activates the D192N mutant *Bh*-RNase H but also reduces the substrate specificity of retroviral RNases H so that dsRNA is cleaved (Hughes et al., 1998).

Attenuation by Metal Ions

E188 is an unexpected fifth carboxylate in the *Bh*-RNase H active site. In the D132N structure, it coordinates the A site metal ion. In the D192N structure, it is replaced by the water molecule coordinated by D132, and its side chain swings out of the active site (Figures 5B and 5C). To investigate its role in catalysis, we made E188Q and E188A substitutions in RNase HC. The behavior of the E188Q mutant protein is indistinguishable from the wild-type RNase HC, but the E188A protein exhibits a reduced nuclease activity (Figure 5E). We speculate that a Glu or Gln at this position provides a transient ligand to facilitate the recruitment and orientation of the A site Mg^{2+}. Interestingly, the E188A mutant RNase HC is resistant to 50 mM Mg^{2+}, whereas the wild-type enzyme is inhibited at this Mg^{2+} concentration (see the Supplemental Data available with this article online). E188 may be responsible for the attenuation by recruiting adventitiously a third metal ion at high concentrations of Mg^{2+} and perturbing the optimal geometry of metal ions at the A and B sites. Structural superposition suggests that H124 of *E. coli* RNase H, which plays an important but nonessential role in catalysis (Oda et al., 1993), may be the equivalent of E188. An Ala substitution of H124 indeed eliminates the metal-dependent attenuation (Keck et al., 1998).

The Two Metal Ions Exchange Roles during DNA Transposition

Two metal ions are also found in the active site of Tn5 transposase complexed with a transposon end (Davies et al., 2000; Steiniger-White et al., 2004). The related Tn5 and Tn10 transposases catalyze four successive chemical reactions during transposition (Figure 6A). Mutagenesis and functional assays indicate that a single active site catalyzes all chemical reactions (Bolland and Kleckner, 1996). Analyses of stereoselectivity of DNA substrates further suggested that "the 3′ end of the transposon remains bound to the same side of the active site" in the first three reaction steps but not the fourth (Kennedy et al., 2000). Even after determination of the crystal structure of a Tn5 transposase-DNA complex trapped after the third reaction step (Davies et al., 2000), how the metal ions in the active site assist the four chemical reactions and how the fourth step is stereochemically different from the other three have not been addressed.

Comparison of the RNase HC and Tn5 structures reveals that the two metal ions occupy similar positions, but the coordination is symmetric in Tn5 transposase and asymmetric in RNase H (Figure 6D). In Tn5, there are only three conserved carboxylates. The first carboxylate coordinates both metal ions; the latter two coordinate either metal in a loosely symmetric fashion. In RNases H, an additional carboxylate (E109 in *Bh*-RNase H and E48 in *E. coli*) coordinates metal B and sequesters it from bulk solvent. Most interestingly, the nucleophilic water in the RNase H structure is nearly superimposable with the 3′-OH at the transposon end, which is the nucleophile for the strand-transfer reaction (step 4, Figure 6A). This 3′-OH is produced from the hairpin intermediate by Tn5 transposase in step 3, where a water molecule attacks the phosphate from the opposite side of the 3′-OH (Figures 6A and 6D). This means that in Tn5 transposase, the metal ion equivalent to the B metal in RNase H activates the water molecule for the hydrolysis (Figure 6D). The metal ion at the A site then coordinates the 3′-OH for the strand-transfer reaction.

We propose that the symmetrically coordinated metal ions in Tn5 transposase alternately activate a water molecule and 3′-OH in successive chemical reactions and that the 3′-OH of the transposon end remains coordinated to the same metal ion throughout the course of transposition. This hypothesis is supported by the alternating stereoselectivity (R_p, S_p, and R_p) of the first three reactions (Kennedy et al., 2000). The altered stereochemical preference in the strand-transfer step (R_p) can be explained by different orientations of target versus donor DNAs. We designate the metal ion activating water as H, for hydrolysis, and the one bound to the 3′-OH as T, for strand transfer (Figure 6D). This alternating usage of the two metal ions is aptly termed a ping-pong mechanism.

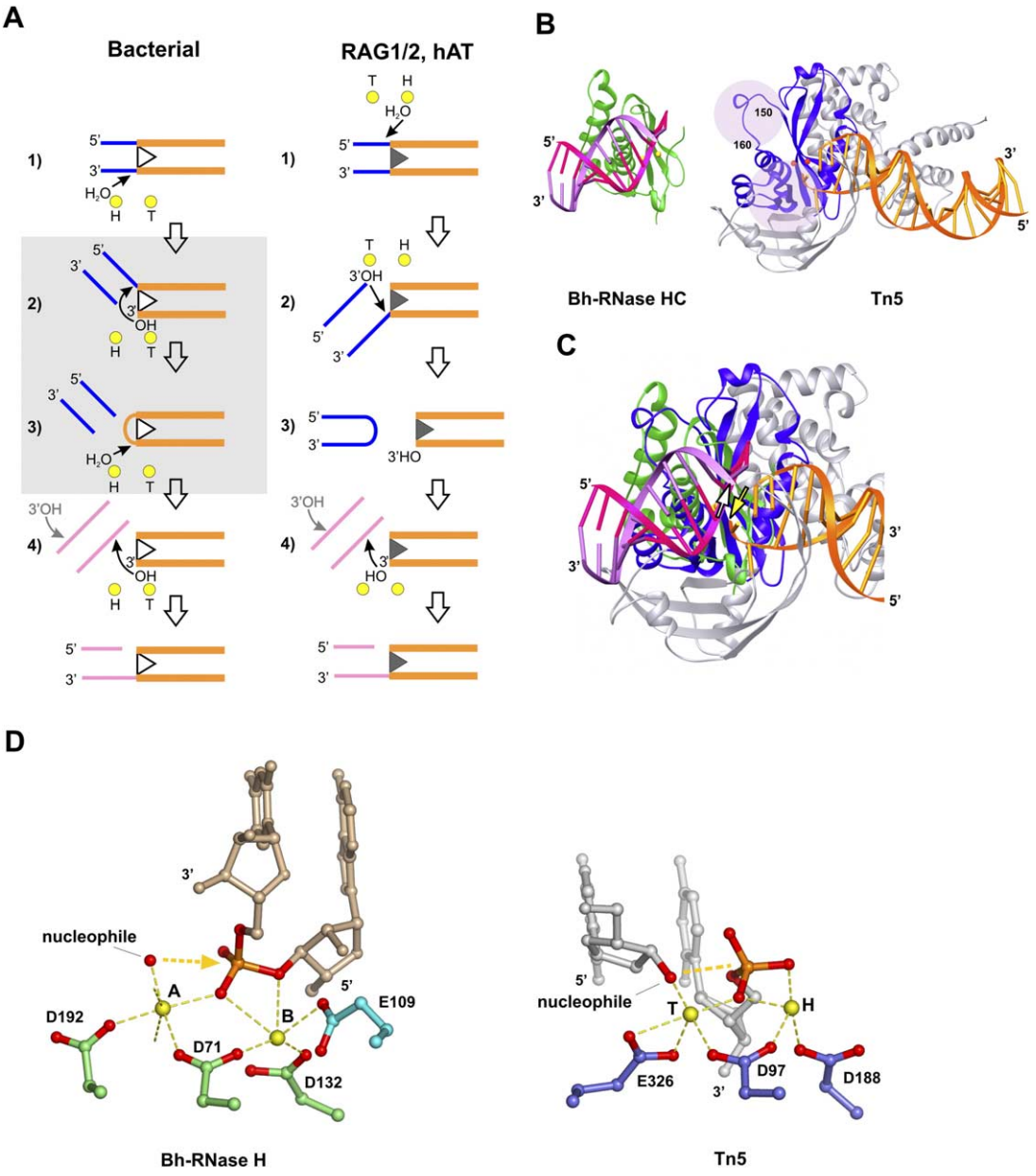

Figure 6. Comparison of RNase H and Transposase

(A) Diagrams of DNA transposition. Bacterial transposition and retroviral integration are shown on the left, and the hAT superfamily and V(D)J recombination in eukaryotes on the right. The transposon DNA is shown in orange, flanking sequence in blue, and target DNA in pink. The H and T metal ions activate the nucleophiles for hydrolysis and strand transfer, respectively. The steps unique to Tn5 and Tn10 transposition are highlighted in gray.

(B) The crystal structures of RNase HC(D132N) and Tn5 (PDB ID code 1MUS) complexed with substrate. The catalytic core in Tn5 is highlighted in blue. The two metal ions are shown as yellow/orange spheres. The regions in Tn5 that may interact with flanking or target DNA are shaded in lilac.

(C) Superposition of the catalytic core of the above two structures. A white arrow represents the polarity of the cleaved strand in RNase HC, and a yellow arrow in Tn5.

(D) The active sites of RNase HC and Tn5 are shown side by side after superposition. The conserved carboxylates, the metal ions, the scissile phosphate, and nucleophile are highlighted and labeled.

Implications for Substrate Binding and Eukaryotic Transposition

Superposition of the RNase H and Tn5 crystal structures reveals that the RNA/DNA hybrid and the transposase substrate overlap only in the active site (Figure 6C). The substrate binding site in RNase H corresponds to a basic region and a disordered but positively charged loop between residues 150 and 160 in Tn5 (Figure 6B), which may interact with flanking or target DNA.

We also notice that the cleavage strand in the RNase

HC structure has opposite polarity (5′→3′ versus 3′→5′) to the substrate in the Tn5 complex (Figure 6C). The conserved active site apparently does not specify the orientation of an RNA or DNA strand. The surrounding elements unique to each enzyme must determine the substrate specificity and its orientation in the active site. Translation of 6–8 Å across the minor groove can alter cleavage from one strand to the other, as the two metal ions are coordinated symmetrically. The ambivalence of strand polarity provides a simple answer to a long-standing puzzle. Eukaryotic transposases, e.g., RAG1/2 and hAT superfamily members, initiate transposition by cleaving the 5′ end of a transposon DNA rather than the 3′ end as do bacterial transposases and retroviral integrase (Figure 6A; Zhou et al., 2004). Since the active site is conserved from bacterial to eukaryotic transposases (Zhou et al., 2004), the two metal ions in eukaryotic enzymes likely also trade roles and alternately catalyze hydrolysis and strand transfer. As the cleavage strand switches its polarity, the T metal in Tn5 transposase probably functions as the H metal in the eukaryotic transposases, and vice versa (Figure 6A).

The switching of the cleavage strand in eukaryotes does lead to complications. Firstly, to free the 3′-OH of a transposon for transposition, cleavage of the second strand via a hairpin intermediate becomes mandatory (Figure 6A). Secondly, the 3′-OH of a flanking DNA is coordinated to the T metal during the first three steps (Figure 6A), but the 3′-OH of a transposon is the nucleophile for the fourth step (strand transfer). Eukaryotic transposases must undergo major conformational changes to recapture the 3′-OH of a transposon end prior to strand transfer. The role of each metal ion in this last step is yet to be defined. Evolution may select transposases that cleave the "wrong" strand of a transposon to reduce transposition efficiency for the sake of genomic stability. In the case of V(D)J recombination, RAG1/2 does not proceed to strand transfer under normal physiological conditions.

The Two-Metal-Ion Catalysis in Holliday Junction Resolvase and RISC Argonaute

RNase H is the founding member of a large family of polynucleotidyl transferases including RNase, DNase, and transposase (integrase). The two-metal-ion catalysis found in RNases H and transposases probably occurs in all members. Besides Tn5, many apoprotein structures from this superfamily have been determined (Rice and Baker, 2001). Two spatially conserved Asps are present from RNase H to Argonaute (Figure 1A). Two additional conserved carboxylates are present in RNase HII as in RNase H, except for the fact that the E109 equivalent migrates from a helix to a strand. The configuration of the active site of RuvC is rather different, although it contains four conserved carboxylates (Ariyoshi et al., 1994; Ceschini et al., 2001). The second spatially conserved Asp is replaced by Glu, and the remaining two carboxylates are both located near the C terminus (Figure 1A). This peculiar geometry suggests that the two metal ions are coordinated differently in RuvC from in RNase H.

In the catalytic domain of Argonaute, a conserved His (H745 in *P. furi*) occupies the same position relative to the two conserved Asps (Parker et al., 2004; Song et al., 2004) as D192 does in RNase H. Our D192N mutant protein, which is active in the presence of Mn^{2+}, indicates that a carboxylamide at this position is partially functional. Histidine, which has chemical functionality overlapping with a carboxylamide, may thus substitute for D192 and coordinate the A site metal ion in Argonaute. For the B site metal coordination, a conserved Glu (E635 in *P. furi*) is in the vicinity of the two conserved Asps and may be functionally equivalent to E109 in *Bh*-RNase H. E635, however, is 4 Å further away from the other three catalytic residues than E109 is and may be too far away to contact the B site metal ion without conformational changes. Alternatively, a nearby conserved Arg (R627) may orient a phosphate, e.g., the one 5′ to the scissile bond, to substitute the requirement for a third carboxylate. With the conserved active-site geometry, we expect the substrate orientation and metal-ion function in Argonaute to be similar to RNase H.

Conclusions

The crystal structures of *Bh*-RNase H reveal that the enzyme recognizes an RNA/DNA hybrid in a mixed A and B conformation unique to hybrid duplexes and targets the RNA strand for cleavage by specific interactions with its 2′-OHs. Two metal ions are found in the active site of RNase H for activating the nucleophile and stabilizing the transition state. They are likely to be present and coordinated by the two spatially conserved Asps in each member of the RNase H-transposase superfamily. A third or fourth carboxylate (histidine in Argonaute) unique to each subfamily determines the geometry of metal-ion coordination and types of catalysis. Positioning of the metal ions depends on the carboxylates and suitable substrate. Efficient catalysis takes place only when the two metal ions are separated by an ideal distance and arranged in appropriate geometry. The highly specific coordination requirement of Mg^{2+} ions contributes to the substrate specificity. Depending on the symmetry of metal-ion coordination, a generally conserved active site may catalyze unidirectional hydrolysis or sequential cleavage and strand transfer by a ping-pong mechanism.

Experimental Procedures

DNA Constructs and Protein Purification

B. halodurans genomic DNA was obtained from Dr. Mitsuhiro Itaya (Keio University, Japan). The full-length RNase H (*rnhA*) and C-terminal fragment were cloned into pET15b vector (Novagen), which contains an N-terminal His_6 tag followed by a thrombin cleavage site. E109Q, D132N, E188Q, E188A, and D192N mutations were made by site-directed mutagenesis using the QuikChange Site-Directed Mutagenesis Kit (Stratagene) and confirmed by sequencing. Protein expression was carried out in BL21 (DE3) pLysS *E. coli* cells at 37°C in LB medium.

Bh-RNase H and RNase HC were purified on a Ni column and eluted in 40 mM NaH_2PO_4 (pH 7.0), 300 mM NaCl, 5% glycerol, 1.4 mM β-mercaptoethanol, and 300 mM imidazole. The buffer was exchanged to 40 mM NaH_2PO_4, 150 mM NaCl, 5% glycerol, 2 mM DTT, and 0.5 mM EDTA for thrombin digestion. The proteins were further purified on a Phenyl Superose column with a 2 to 0.3 M gradient of ammonium sulfate, concentrated to 15–20 mg/ml, and stored in 20 mM HEPES (pH 7.0), 75 mM NaCl, 5% glycerol, 0.5 mM EDTA, 2 mM DTT at 4°C or −20°C. Selenomethionine-labeled (SeMet) RNase HC(D132N) was expressed using methionine-auxo-

trophic *E. coli* strain B834 (DE3) pLysS in a defined medium (Hendrickson et al., 1990) and purified using a similar protocol.

RNase H-Activity Assays

The activity of native and mutant proteins were assayed using a 5′-^{32}P-labeled 12-mer RNA/DNA or uniformly labeled poly(rA)/poly(dT) in 50 mM Tris-HCl (pH 7.9), 50 mM NaCl, 5 mM $MgCl_2$ (or 20 mM $MnCl_2$), 1 mM DTT, 20 μg/ml BSA, and 4% glycerol. Aliquots of reaction mixtures were taken and analyzed on a 12% TBE polyacrylamide gel. The reaction products were visualized by autoradiography.

Substrate Binding Assay

Substrate binding was assayed using gel filtration. Wild-type or mutant RNase HC (1 mg/ml) was mixed with a 12-mer RNA/DNA hybrid or dsRNA and dsDNA of equivalent sequences at 2:1 molar ratio in 20 mM HEPES (pH 7.5), 75 mM NaCl, 5% glycerol, 2 mM DTT, and 5 mM $MgCl_2$ (mutant proteins) or 0.5 mM EDTA (wild-type). After incubation at room temperature for 5 min, the mixture (50 μl) was applied to a Superdex 75 HR 10/30 FPLC column (Pharmacia/GE Healthcare). The D132N protein complexed with RNA/DNA hybrids was eluted before the protein and substrate. When the 2:1 molar ratio was slightly varied, additional peaks of excess protein or substrate appeared. No complex peak was observed with the dsRNA or dsDNA or when wild-type, E109Q, or D192N replaced D132N RNase HC.

Crystallization

SeMet and native RNase HC(D132N) (8 mg/ml) were mixed at equal volume with the reservoir solution (30% PEG 2000 monomethyl ether, 0.2 M ammonium sulfate, and 0.1 M sodium acetate [pH 4.6]) and crystallized by sitting drop vapor diffusion method at 4°C. The crystals were transferred to cryosolution containing 35% PEG 2000 MM and 10% glycerol before freezing in liquid nitrogen for data collection.

RNA (5′-GACACCUGAUUC-3′) and DNA (5′-GAATCAGGTGTC-3′) were purchased from Yale University (http://keck.med.yale.edu). The RNA was deprotected using 1 M solution of tetrabutylammonium fluoride in THF, and the oligonucleotide was purified using OPC cartridge (Applied Biosystems). The DNA was purified using a reverse-phase R3 column (Applied Biosystems). The RNA and DNA were annealed and mixed with the protein at 2:1 molar ratio in the presence of 5 mM $MgCl_2$. The final protein concentration in the mixture was 10 mg/ml. The D132N complex crystals were obtained using the sitting drop vapor diffusion method against 20% MPD, 0.2 M NaCl, and 0.1 M HEPES (pH 7.5) at 21°C. Cocrystals of D192N protein and RNA/DNA were obtained using the same method with reservoir containing 5% ethanol, 0.35 M NaCl, and 0.1 M Tris (pH 7.0). Both cocrystals were cryoprotected by 35% MPD and flash frozen in liquid nitrogen.

Data Collection and Structure Determination

X-ray diffraction data were collected at ID-22 and BM-22 beamlines in Advanced Photon Source on a Mar225 or Mar300 CCD detector. A three-wavelength dataset was collected from a single crystal of SeMet RNase HC(D132N). The crystal belongs to the $P3_121$ space group with one protein molecule per asymmetric unit and diffracted to 1.8 Å at 100 K (Table 1). The data sets were processed and scaled using HKL2000 (Otwinowski and Minor, 1997). The single selenium site was found using SOLVE (Terwilliger and Berendzen, 1999), and 86% of the polypeptide chain was automatically traced using RESOLVE. The model was manually completed using O (Jones et al., 1991). Refinement was carried out using CNS (Brunger et al., 1998) with a 1.5Å dataset collected on the native protein. Table 1 shows the statistics for the final model, which consists of residues 62–193 and 232 water molecules.

Crystals of D132N and D192N RNase HC complexed with the RNA/DNA hybrid diffracted X-rays to 1.85 and 2.2 Å, respectively. The data were processed and scaled using HKL2000, and the structures were solved by molecular replacement using the apoprotein structure and EPMR software (Kissinger et al., 1999). The electron densities for the nucleic acids were obvious, and the model was manually built and refined using CNS and O. The final models contained a 12-mer hybrid and two protein molecules (I and II). In the D132N crystal, residues 62–196 are traced in I and 59–194 in II; in the D192N crystal, residues 61–193 are traced in both molecules. In both crystals, the RNA/DNA hybrids are stacked end to end, forming a continuous fiber, and protein-protein contacts crosslink neighboring complexes, thus forming the crystal lattices. In the crystals of the D192N complex, the 12-mer substrate is bound to each protein molecule at two equivalent positions 6 bp apart. Therefore, two substrate models were refined as alternative conformations with 50% occupancy. Noncrystallographic symmetry (NCS) was applied with low stringency for protein and high stringency for the RNA/DNA hybrids.

The nucleic-acid conformation was analyzed using the program CURVES (Lavery and Sklenar, 1988). Structural comparison and analyses were done using O (Jones et al., 1991) or MolMol (http://hugin.ethz.ch/wuthrich/software/molmol/). Figures were prepared using Ribbons (Carson, 1991) and Pymol (http://pymol.sourceforge.net/).

Supplemental Data

Supplemental Data include one figure and are available with this article online at http://www.cell.com/cgi/content/full/121/7/1005/DC1/.

Acknowledgments

We thank Drs. J.Y. Lee and S. Ramon-Maiques for help with data collection and structure determination. We are also indebted to Drs. S. Cerritelli, M. Gellert, K. Mizuuchi, and D. Leahy for insightful comments.

Received: March 4, 2005
Revised: April 7, 2005
Accepted: April 19, 2005
Published: June 30, 2005

References

Ariyoshi, M., Vassylyev, D.G., Iwasaki, H., Nakamura, H., Shinagawa, H., and Morikawa, K. (1994). Atomic structure of the RuvC resolvase: a holliday junction-specific endonuclease from E. coli. Cell *78*, 1063–1072.

Arudchandran, A., Cerritelli, S., Narimatsu, S., Itaya, M., Shin, D.Y., Shimada, Y., and Crouch, R.J. (2000). The absence of ribonuclease H1 or H2 alters the sensitivity of Saccharomyces cerevisiae to hydroxyurea, caffeine and ethyl methanesulphonate: implications for roles of RNases H in DNA replication and repair. Genes Cells *5*, 789–802.

Bolland, S., and Kleckner, N. (1996). The three chemical steps of Tn10/IS10 transposition involve repeated utilization of a single active site. Cell *84*, 223–233.

Broccoli, S., Rallu, F., Sanscartier, P., Cerritelli, S.M., Crouch, R.J., and Drolet, M. (2004). Effects of RNA polymerase modifications on transcription-induced negative supercoiling and associated R-loop formation. Mol. Microbiol. *52*, 1769–1779.

Brunger, A.T., Adams, P.D., Clore, G.M., DeLano, W.L., Gros, P., Grosse-Kunstleve, R.W., Jiang, J.S., Kuszewski, J., Nilges, M., Pannu, N.S., et al. (1998). Crystallography & NMR system: A new software suite for macromolecular structure determination. Acta Crystallogr. D Biol. Crystallogr. *54*, 905–921.

Carson, M. (1991). Ribbons 2.0. J. Appl. Crystallogr. *24*, 958–961.

Cerritelli, S.M., Frolova, E.G., Feng, C., Grinberg, A., Love, P.E., and Crouch, R.J. (2003). Failure to produce mitochondrial DNA results in embryonic lethality in Rnaseh1 null mice. Mol. Cell *11*, 807–815.

Ceschini, S., Keeley, A., McAlister, M.S., Oram, M., Phelan, J., Pearl, L.H., Tsaneva, I.R., and Barrett, T.E. (2001). Crystal structure of the fission yeast mitochondrial Holliday junction resolvase Ydc2. EMBO J. *20*, 6601–6611.

Davies, D.R., Goryshin, I.Y., Reznikoff, W.S., and Rayment, I. (2000).

Three-dimensional structure of the Tn5 synaptic complex transposition intermediate. Science *289*, 77–85.

Goedken, E.R., and Marqusee, S. (2001). Co-crystal of Escherichia coli RNase HI with Mn2+ ions reveals two divalent metals bound in the active site. J. Biol. Chem. *276*, 7266–7271.

Gotte, M., Fackler, S., Hermann, T., Perola, E., Cellai, L., Gross, H.J., Le Grice, S.F., and Heumann, H. (1995). HIV-1 reverse transcriptase-associated RNase H cleaves RNA/RNA in arrested complexes: implications for the mechanism by which RNase H discriminates between RNA/RNA and RNA/DNA. EMBO J. *14*, 833–841.

Haren, L., Ton-Hoang, B., and Chandler, M. (1999). Integrating DNA: transposases and retroviral integrases. Annu. Rev. Microbiol. *53*, 245–281.

Haruki, M., Noguchi, E., Kanaya, S., and Crouch, R.J. (1997). Kinetic and stoichiometric analysis for the binding of Escherichia coli ribonuclease HI to RNA-DNA hybrids using surface plasmon resonance. J. Biol. Chem. *272*, 22015–22022.

Haruki, M., Tsunaka, Y., Morikawa, M., Iwai, S., and Kanaya, S. (2000). Catalysis by Escherichia coli ribonuclease HI is facilitated by a phosphate group of the substrate. Biochemistry *39*, 13939–13944.

Hendrickson, W.A., Horton, J.R., and LeMaster, D.M. (1990). Selenomethionyl proteins produced for analysis by multiwavelength anomalous diffraction (MAD): a vehicle for direct determination of three-dimensional structure. EMBO J. *9*, 1665–1672.

Huang, H., Chopra, R., Verdine, G.L., and Harrison, S.C. (1998). Structure of a covalently trapped catalytic complex of HIV-1 reverse transcriptase: implications for drug resistance. Science *282*, 1669–1675.

Hughes, S.H., Arnold, E., and Hostomsky, Z. (1998). RNase H of retroviral reverse transcriptases. In Ribonucleases H, R.J. Crouch and J.J. Toulme, eds. (Paris: INSERM), pp. 195–224.

Jones, T.A., Zou, J.Y., and Cowan, S.W. (1991). Improved methods for building protein models in electron density maps and the location of errors in these models. Acta Crystallogr. A *47*, 110–119.

Julias, J.G., McWilliams, M.J., Sarafianos, S.G., Arnold, E., and Hughes, S.H. (2002). Mutations in the RNase H domain of HIV-1 reverse transcriptase affect the initiation of DNA synthesis and the specificity of RNase H cleavage in vivo. Proc. Natl. Acad. Sci. USA *99*, 9515–9520.

Kanaya, S. (1998). Enzymatic activity and protein stability of *E. coli* ribonuclease HI. In Ribonucleases H, R.J. Crouch and J.J. Toulme, eds. (Paris: INSERM), pp. 1–38.

Katayanagi, K., Miyagawa, M., Matsushima, M., Ishikawa, M., Kanaya, S., Ikehara, M., Matsuzaki, T., and Morikawa, K. (1990). Three-dimensional structure of ribonuclease H from E. coli. Nature *347*, 306–309.

Keck, J.L., Goedken, E.R., and Marqusee, S. (1998). Activation/attenuation model for RNase H. A one-metal mechanism with second-metal inhibition. J. Biol. Chem. *273*, 34128–34133.

Kennedy, A.K., Haniford, D.B., and Mizuuchi, K. (2000). Single active site catalysis of the successive phosphoryl transfer steps by DNA transposases: insights from phosphorothioate stereoselectivity. Cell *101*, 295–305.

Kissinger, C.R., Gehlhaar, D.K., and Fogel, D.B. (1999). Rapid automated molecular replacement by evolutionary search. Acta Crystallogr. D Biol. Crystallogr. *55*, 484–491.

Kogoma, T., and Foster, P.L. (1998). Physiological functions of *E. coli* RNase HI. In Ribonucleases H, R.J. Crouch and J.J. Toulme, eds. (Paris: INSERM), pp. 39–66.

Kopka, M.L., Lavelle, L., Han, G.W., Ng, H.L., and Dickerson, R.E. (2003). An unusual sugar conformation in the structure of an RNA/DNA decamer of the polypurine tract may affect recognition by RNase H. J. Mol. Biol. *334*, 653–665.

Krakowiak, A., Owczarek, A., Koziolkiewicz, M., and Stec, W.J. (2002). Stereochemical course of Escherichia coli RNase H. ChemBioChem *3*, 1242–1250.

Lai, L., Yokota, H., Hung, L.W., Kim, R., and Kim, S.H. (2000). Crystal structure of archaeal RNase HII: a homologue of human major RNase H. Struct. Fold. Des. *8*, 897–904.

Lavery, R., and Sklenar, H. (1988). The definition of generalized helicoidal parameters and of axis curvature for irregular nucleic acids. J. Biomol. Struct. Dyn. *6*, 63–91.

Lovell, S., Goryshin, I.Y., Reznikoff, W.R., and Rayment, I. (2002). Two-metal active site binding of a Tn5 transposase synaptic complex. Nat. Struct. Biol. *9*, 278–281.

Oda, Y., Yoshida, M., and Kanaya, S. (1993). Role of histidine 124 in the catalytic function of ribonuclease HI from Escherichia coli. J. Biol. Chem. *268*, 88–92.

Ohtani, N., Haruki, M., Morikawa, M., Crouch, R.J., Itaya, M., and Kanaya, S. (1999). Identification of the genes encoding Mn2+-dependent RNase HII and Mg2+-dependent RNase HIII from Bacillus subtilis: classification of RNases H into three families. Biochemistry *38*, 605–618.

Otwinowski, Z., and Minor, W. (1997). Processing of X-ray diffraction data collected in oscillation mode. In Methods in Enzymology, C.W. Carter and R.M. Sweet, eds. (New York: Academic Press), pp. 307–326.

Parker, J.S., Roe, S.M., and Barford, D. (2004). Crystal structure of a PIWI protein suggests mechanisms for siRNA recognition and slicer activity. EMBO J. *23*, 4727–4737.

Repaske, R., Hartley, J.W., Kavlick, M.F., O'Neill, R.R., and Austin, J.B. (1989). Inhibition of RNase H activity and viral replication by single mutations in the 3′ region of Moloney murine leukemia virus reverse transcriptase. J. Virol. *63*, 1460–1464.

Rice, P.A., and Baker, T.A. (2001). Comparative architecture of transposase and integrase complexes. Nat. Struct. Biol. *8*, 302–307.

Sarafianos, S.G., Das, K., Tantillo, C., Clark, A.D., Jr., Ding, J., Whitcomb, J.M., Boyer, P.L., Hughes, S.H., and Arnold, E. (2001). Crystal structure of HIV-1 reverse transcriptase in complex with a polypurine tract RNA:DNA. EMBO J. *20*, 1449–1461.

Song, J.J., Smith, S.K., Hannon, G.J., and Joshua-Tor, L. (2004). Crystal structure of Argonaute and its implications for RISC slicer activity. Science *305*, 1434–1437.

Steiniger-White, M., Rayment, I., and Reznikoff, W.S. (2004). Structure/function insights into Tn5 transposition. Curr. Opin. Struct. Biol. *14*, 50–57.

Steitz, T.A., and Steitz, J.A. (1993). A general two-metal-ion mechanism for catalytic RNA. Proc. Natl. Acad. Sci. USA *90*, 6498–6502.

Terwilliger, T.C., and Berendzen, J. (1999). Automated MAD and MIR structure solution. Acta Crystallogr. D Biol. Crystallogr. *55*, 849–861.

Tisdale, M., Schulze, T., Larder, B.A., and Moelling, K. (1991). Mutations within the RNase H domain of human immunodeficiency virus type 1 reverse transcriptase abolish virus infectivity. J. Gen. Virol. *72*, 59–66.

Tsunaka, Y., Takano, K., Matsumura, H., Yamagata, Y., and Kanaya, S. (2005). Identification of single Mn(2+) binding sites required for activation of the mutant proteins of E.coli RNase HI at Glu48 and/or Asp134 by X-ray crystallography. J. Mol. Biol. *345*, 1171–1183.

Wu, H., Lima, W.F., Zhang, H., Fan, A., Sun, H., and Crooke, S.T. (2004). Determination of the role of the human RNase H1 in the pharmacology of DNA-like antisense drugs. J. Biol. Chem. *279*, 17181–17189.

Yang, W., Hendrickson, W.A., Crouch, R.J., and Satow, Y. (1990). Structure of ribonuclease H phased at 2 A resolution by MAD analysis of the selenomethionyl protein. Science *249*, 1398–1405.

Zhou, L., Mitra, R., Atkinson, P.W., Hickman, A.B., Dyda, F., and Craig, N.L. (2004). Transposition of hAT elements links transposable elements and V(D)J recombination. Nature *432*, 995–1001.

Accession Numbers

Coordinates have been deposited in the Protein Data Bank with the ID codes 1ZBF for apo RNase HC(D132N), 1ZBI for RNase HC(D132N) in complex with the hybrid, and 1ZBL for the RNase HC(D192N) complex.